Effect of the Size and Amount of ZrO_2 Addition on Properties of $SrCo_{0.4}Fe_{0.6}O_{3-\delta}$

Li Yang, Liang Tan, Xuehong Gu, Hong Qi, Wanqin Jin, Lixiong Zhang, and Nanping Xu
Membrane Science & Technology Research Center, Nanjing University of Technology, Nanjing 210009, P.R. China

The effects of ZrO_2 addition with various particle sizes (1, 3, and 56 μm) and various amounts (0, 1, 3, 5, 7, 9 wt. %) on structure, oxygen permeation, and stability of $SrCo_{0.4}Fe_{0.6}O_{3-\delta}$ (SCF) were investigated. XRD and EDX analysis revealed that the dissolution of Zr cation into the B site of SCF phase occurred with the addition of ZrO_2, resulting in a lattice expansion of SCF at elevated temperatures. The dissolution amount of Zr in the SCF phase increased with a decrease of ZrO_2 particle size and an increase in the amount of ZrO_2 added, and, therefore, resulted in a decrease of oxygen permeation flux of the membranes and an increase in their structural stability in a helium atmosphere. This study indicated that adding a certain amount of Zr cation in SCF oxide was an effective route to sustain the structural stability of SCF in low oxygen partial pressure, and the optimum ZrO_2 addition was 3 wt.% with a particle size of 1 μm, which greatly improved the structural stability without significantly changing the oxygen permeability of SCF.

Introduction

The potential application of mixed conductors exhibited both oxide ion and electron conduction, as oxygen separation membranes and catalysts have stimulated interests in developing new materials and optimizing known materials in recent years (Lu et al., 2000; Kharton et al., 2000; Prado et al., 2002). The main advantages of such membranes are related to an infinite theoretical permselectivity with respect to oxygen, caused by the only possible mechanism of oxygen transport, that is, oxygen ion hopping between neighboring vacant sites in the crystal lattice. Also, technologies for partial oxidation of methane (POM) based on mixed conductors can combine the oxygen separation and partial oxidation in one operation, thereby eliminating a costly oxygen separation plant that is needed in the traditional POM units (Foster et al., 1998).

One of the most promising groups of mixed conductors is the perovskite oxides having high ionic conductivity with prevailing electronic conductivity (Kharton et al., 1996; Stevenson et al., 1996; Tsai et al., 1998). Perovskite-type oxides, such as La(Sr)Co(Fe)$O_{3-\delta}$ compositions, were tested successfully under various external conditions (Balachandran et al., 1995; ten Elshof et al., 1995; Xu and Thomson, 1997; Zeng et al., 1998). However, the application of mixed-conductive membranes is often limited by specific disadvantages of the membrane materials known at the present time, for instance, the order–disorder phase transition in the oxygen sublattice (Qiu et al., 1995; Liu et al., 1996; Kruidhof et al., 1993). The transition from a high-temperature structure, in which the oxygen vacancies are disordered, to a low-temperature phase, in which the vacancies are highly ordered, leading to a reduction in oxygen ion mobility. Such a transition is characteristic of most perovskites derived from the strontium cobaltite $SrCoO_{3-\delta}$ (Kruidhof et al., 1993). In addition, a high oxygen chemical potential gradient in the Sr(Co, Fe)$O_{3-\delta}$-type membranes results in a crystal lattice mismatch inside the ceramic, leading to the fracture of the membranes (Pei et al., 1995). Thus, the disadvantages of $SrCoO_{3-\delta}$-based ceramics create a necessity to develop new materials and optimize known materials for oxygen separation and catalytic membrane reactors. Unfortunately, there is a tendency that high reduction stability likewise correlates with low ionic conductivity and oxygen permeability, simply because the ionic migration requires weakly bonded ions (Weppner, 1992).

Recently, a novel perovskite-related oxide membrane, which was prepared by the addition of ZrO_2 into $SrCo_{0.4}Fe_{0.6}$-$O_{3-\delta}$ (SCF), was reported in our laboratory (Li

Correspondence concerning this article should be addressed to N. Xu.

et al., 1999; Yang et al., 2002). The oxygen nonstoichiometry, transport properties, and structural stability of ZrO_2-promoted $SrCo_{0.4}Fe_{0.6}O_{3-\delta}$ (SCFZ, ZrO_2 9 wt. % in SCFZ) have been investigated. This investigation revealed that the structure and thermochemical stability of SCF was greatly improved with the addition of ZrO_2, but the oxygen permeation flux was slightly reduced. Since the addition of ZrO_2 has a great effect on the oxygen permeation and the stability of SCF, an understanding of the effects of some factors, such as ZrO_2 particle sizes and the amount of added ZrO_2, and so on, on the properties of the materials becomes very important in the search for better materials for oxygen-permeable dense membranes. The aim of the present work is to investigate these factors on the structure, oxygen permeation, and the stability of SCFZ oxides in a search for a suitable composition exhibiting high oxygen flux as well as structure stability in reducing atmosphere.

Experimental Studies

Sample preparation

In this study, two methods were used to prepare SCFZ powders by adding different particle sizes of ZrO_2. For method I, SCF powder was first prepared using $SrCO_3$ (99.9%), Co_2O_3 (99.9%), and Fe_2O_3 (99.9%) by the solid-state reaction method (Yang et al., 2002), then mixed powders with average particle sizes of 56 μm, 3 μm, and 1 μm (Stanford Materials Corporation, San Mateo, CA), respectively, with ZrO_2 in ethanol by a motor agitator. The obtained mixtures were then calcined at 1223 K for 4 h and finally uniaxially pressed into disks with an oil pressure of 200 MPa and sintered at 1473 K for 5 h. For method II, the required amounts of $SrCO_3$, Co_2O_3, Fe_2O_3, and ZrO_2 were directly mixed by a motor agitator, then calcined at 1,223 K for 4 h and uniaxially pressed into disks and sintered at 1,473 K for 5 h. The amount of ZrO_2 added, was 9 wt. % in SCFZ in both methods. The sintered disks were found to have densities $>92\%$ of the theoretical density. The short notions of the samples with different sizes of ZrO_2 additions are given in Table 1. SCFZ added with different amounts (0, 1, 3, 5, 7, and 9 wt. %) of ZrO_2 was prepared by method II, as just described using ZrO_2 with a particle size of 1 μm.

Characterization

The phase distributions in the synthesized powders and sintered membranes were determined by X-ray diffraction (XRD, Bruker D8 Advance). Sintered membranes were prepared for XRD by grinding the samples by a mortar in a pestle. The experimental diffraction patterns were collected at room temperature by step scanning in the range of $15 \le 2\theta \le 90°$ in 0.02° increments. The X-ray data were used to calculate the lattice parameters. Structure changes of the samples under reducing conditions were also studied by XRD. Samples were equilibrated at various temperatures in helium and then cooled to room temperature under the same atmosphere. The obtained powders were immediately examined by XRD. Scanning electron microscopy (SEM) and energy-dispersive X-ray (EDX) analysis were performed using a JSM 6300 scanning microscope equipped with a Sigma energy-dispersive X-ray microanalysis system. SEM images were recorded in back-scattered electron modes. Thermogravimetric analysis (TG) and differential scanning calorimetry analysis (DSC) were performed using NETZSCH STA 409 PC in the range of 273 K to 1,273 K at heating and cooling rates of 10 K/min in pure nitrogen atmosphere.

Table 1. Short Notations of Samples Added with Different Sizes of ZrO_2

Short Notation	Samples
I-1 M	ZrO_2 addition with 1 μm by method I
I-3 M	ZrO_2 addition with 3 μm by method I
I-56 M	ZrO_2 addition with 56 μm by method I
II-1 M	ZrO_2 addition with 1 μm by method II
II-3 M	ZrO_2 addition with 3 μm by method II
II-56 M	ZrO_2 addition with 56 μm by method II

Oxygen permeation measurements were performed using a permeation apparatus reported before (Yang et al., 2002). Membrane disks were sealed between two gold rings. Before beginning the oxygen permeation measurement, the assembly was heated to 1,313 K and held for 4 h to form the bonding. One side of the membrane was exposed to air ($P_h = 0.209$ atm) at a flow rate of 200 mL/min^{-1}, while the other side was exposed to a lower oxygen partial pressure (P_{O_2}) that was controlled by regulating the He flow rate by mass flow controllers (Models D07/ZM, Beijing Jianzhong Machine Factory, China). A gas chromatograph (GC, Model Shimabzu GC-7A) equipped with a 5-Å molecule sieve column was connected to the exit of the sweep side. The amount of oxygen passing through the membrane was calculated from the measured outlet flow rate and the oxygen content.

Results and Discussion

Effect of ZrO_2 particle sizes on structure

XRD patterns of the synthesized powders added with different sizes of ZrO_2 prepared by method I revealed that a pure-phase cubic perovskite structure with a lattice parameter $a = 3.863$ Å was formed for SCF. For powders added with ZrO_2, reaction product $SrZrO_3$ was detected in addition to the major component SCF phase, and the extent of its formation was reduced as the ZrO_2 particle sizes increased. In addition, a small amount of unreacted ZrO_2 phase also existed in I-3 M and I-56 M. XRD patterns of sintered I-1 M, I-3 M, and I-56 M membranes are shown in Figure 1. No ZrO_2 phase was detected by XRD for the 1,473 K-sintered membranes, indicating that ZrO_2 was completely reacted with perovskite at high temperatures. However, a trace of cobalt oxides Co_3O_4 was detected by XRD, which may result from the dissolution of Zr cation in the SCF lattice, as stated below. XRD results of samples prepared by method II showed the similar trends. But the extent of reaction between SCF and ZrO_2 for samples prepared by method II was larger than samples prepared by method I. For example, the XRD patterns of I-3M powder calcined at 1223 K showed the existence of ZrO_2 phase, whereas no ZrO_2 was detected in II-3M sample.

Unit-cell dimensions for the SCF phase with different sizes of ZrO_2 were added, and the phase contents obtained from XRD are shown in Table 2. It shows that the lattice parameters of the SCF phase for all the 1,473 K–calcined membranes were estimated to be larger than those of the pure

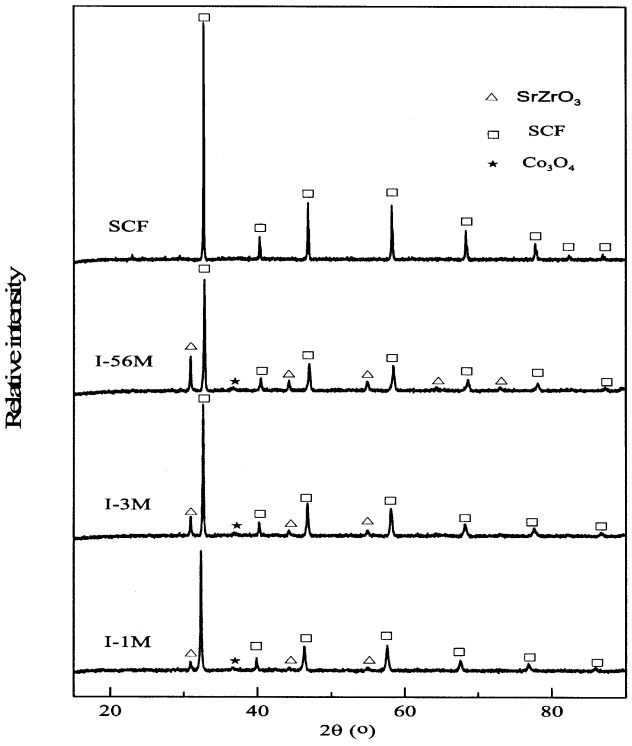

Figure 1. XRD patterns of sintered membranes of I-1 M, I-3 M, and I-56 M.

SCF phase, and it increased with a decrease in ZrO_2 particle size. Figure 2 shows the effect of sintering temperatures on the lattice of the SCF phase with ZrO_2 added (sample I-3 M was used). As could be seen, the lattice parameter of the SCF phase was virtually temperature dependent and it increased directly with the sintering temperatures.

The expansion of the SCF lattice may be due to compositional changes in the SCF phase, originating from the diffusion of cations into SCF. In order to understand the nature of lattice expansion and to determine the phase distribution and its chemistry, we performed the SEM-EDX analyses for the I-1 M, I-3 M, and I-56 M membranes. The results are

Table 2. Lattice Parameters for SCF Phase and Phase Contents for Samples Added with Different Sizes of ZrO_2

Samples	Sintering Temperature (K)	Unit-Cell Parameters a (Å)	Phase Contents
I-1 M	1,223	3.862	P+S
I-3 M	1,223	3.859	P+S+Z
I-56 M	1,223	3.857	P+S+Z
II-1 M	1,223	3.867	P+S+C
II-3 M	1,223	3.862	P+S+C
II-56 M	1,223	3.852	P+S+Z+C
I-1 M	1,473	3.898	P+S+C
I-3 M	1,473	3.885	P+S+C
I-56 M	1,473	3.865	P+S+C
II-1 M	1,473	3.899	P+S+C
II-3 M	1,473	3.885	P+S+C
II-56 M	1,473	3.866	P+S+C

Note: P: Perovskite; S: $SrZrO_3$; Z: ZrO_2; C: Co_3O_4.

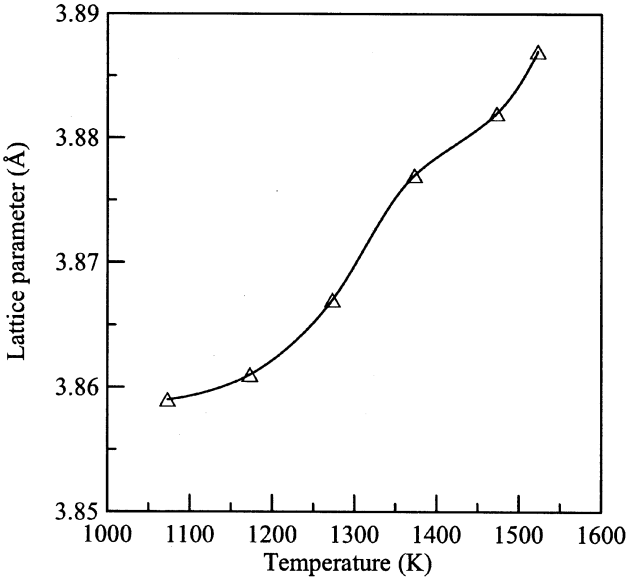

Figure 2. Temperature dependence of lattice parameter for the SCF phase of I-3 M sample.

shown in Figure 3. Two distinct second phases were observed in each sample. EDX indicated that the white phase was rich in Sr, Zr, and O, which was assumed to be the $SrZrO_3$ phase detected by XRD. The dark second phase was rich in Co and O, which was presumably Co_3O_4 detected by XRD. Element analysis of the SCF phase composition (gray areas) of I-1 M, I-3 M, and I-56 M membranes (Table 3) were all found to contain Zr, indicating that diffusion of Zr into the perovskite occurred. The ratio between Sr, Co, Fe, and Zr in the three membranes is 1:0.31:0.78:0.16, 1:0.31:0.83:0.12, and 1:0.41:0.83:0.04, respectively, which indicated that the Zr content in the SCF phase decreased with an increase in ZrO_2 particle size. It was clear that the trend of lattice expansion as a function of ZrO_2 particle size was the same as that of the Zr content in the SCF phase as a function of ZrO_2 particle size. We therefore proposed that the major reason for the expansion of the lattice in the SCF phase when exposed to ZrO_2 and calcined at 1,473 K was the dissolution of Zr cation in the B site of SCF because of the larger ionic radius of Zr^{4+} ($r_{Zr^{4+}} = 0.84$ Å) than those of Co^{3+} ($r_{Co^{3+}} = 0.61$ Å) and Fe^{3+} ($r_{Fe^{3+}} = 0.645$ Å) (Shannon and Prewitt, 1969). The increasing content of Zr cation in the B sites with decreasing ZrO_2 particle size resulted in an increase in the lattice parameters. The solubility of Zr in the B site of $La_{0.7}Sr_{0.3}MnO_3$ (LSM) when exposed to Y_2O_3-stabilized ZrO_2 (YSZ), leading to the expansion of the LSM lattice have been reported by Wiik et al. (1999).

It should be noticed that lattice parameters of the 1,223 K–calcined powders were lower than those of pure-phase SCF (Table 2). The explanation could be described as follows. As mentioned earlier, ZrO_2 reacted with SCF at elevated temperatures. The precipitation of Sr, with a larger ionic radius, from perovskite crystal would result in a lattice contraction. When calcined at 1,223 K, the contraction behavior due to Sr precipitation dominated the expansion behavior of Zr dissolution. As temperatures rose, the amount of Zr dissolution increased (see Figure 3). So at 1,473 K, the

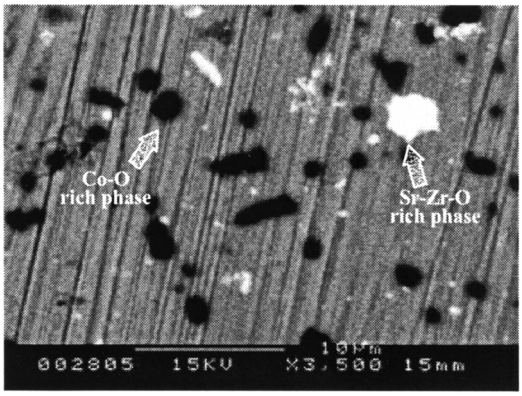

(a)

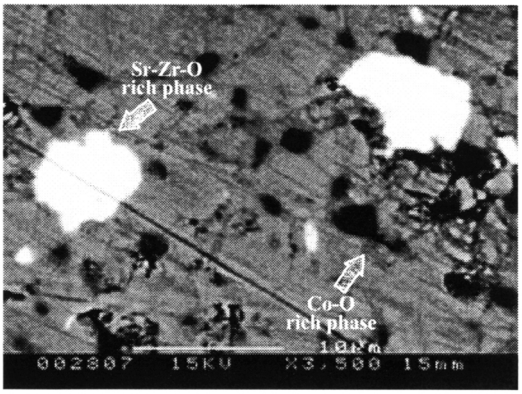

(b)

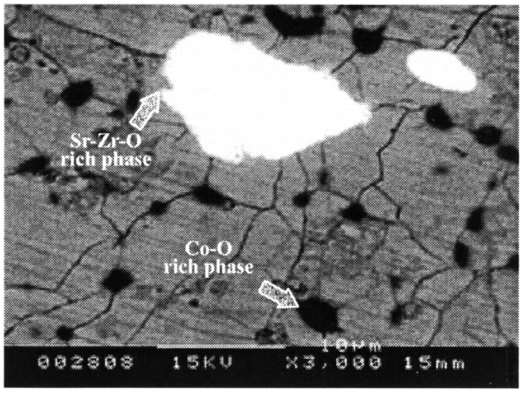

(c)

Figure 3. Back-scattered electron SEM images of (a) I-1 M; (b) I-3 M; and (c) I-56 M membranes.

effect of Zr dissolution was predominant, and, therefore, led to a lattice expansion of the SCF phase. The precipitation of Sr and dissolution of Zr were coincident when the mixture was calcined at elevated temperatures, so the calculation of the amount of dissolved Zr was very difficult. Since the lattice parameter of the SCF phase was closely associated with the Zr content in the SCF phase, in this study we used the lattice parameter of the SCF phase to represent the amount of Zr dissolution. A more detailed study on the solution limit of Zr in the SCF phase of the Sr-Co-Fe-Zr-O system will be published elsewhere.

Table 3. EDX Analysis of SCF Phases for the SCFZ Membranes Added with Different Sizes of ZrO_2

	Composition (mol %)			
Samples	Sr	Co	Fe	Zr
I-1 M	44.55	13.76	34.71	6.98
I-3 M	44.33	13.62	36.82	5.23
I-56 M	43.91	17.98	36.53	1.59

Effect of ZrO_2 particle sizes on oxygen permeation

The temperature dependence of oxygen permeation fluxes through SCF and SCFZ membranes prepared by method I, with different ZrO_2 particle sizes added, is shown in Figure 4. The helium flow rate at the sweep side was kept constant at 30 mL/min, and the oxygen partial pressure at the sweep side varies between 0.009 atm and 0.004 atm, depending on the oxygen permeation rates. It could be seen that oxygen fluxes decreased with the addition of ZrO_2 and they decreased with decreasing ZrO_2 particle sizes. Correlation of oxygen fluxes with the lattice parameters of the SCF phase revealed that the oxygen fluxes decreased with an increase in the SCF lattice. Since the increase of lattice parameters was due to the increasing amount of Zr cation dissolution, we proposed that oxygen fluxes decreased as the increasing content of Zr cation increased in the B site of SCF. From Table 2, we could see that the lattice parameters were close for the 1473 K–sintered membranes prepared by the two methods, but added with the same ZrO_2 sizes. From the preceding results, we postulated that the oxygen fluxes of membranes added with the same size as ZrO_2 prepared by different methods should also be close. Figure 5 shows a comparison of oxygen permeation fluxes of membranes prepared by different methods. Very close oxygen permeation fluxes were found for membranes added that were the same size as ZrO_2, which agreed with the previously mentioned results. Solid solution of Zr in the B sites of SCF increased the M-O bonding energy and reduced the concentration of oxide ion vacancies, both leading to a decrease in oxygen permeability. A decrease in oxygen-ion conductivity with the doping of ZrO_2 in $LaInO_3$ was reported by He et al. (2001).

Since the presence of the second-phase $SrZrO_3$ might also be unfavorable to oxygen permeation due to its lower conductivity than YSZ (Poulsen and van der Puil, 1992), a semiquantitative representation of the relative amount of $SrZrO_3$ in the I-1 M, I-3 M, and I-56 M membranes was obtained using the ratio between the intensity values of 100% reflections for $SrZrO_3$ and SCF. The result is shown in Figure 6. The amount of $SrZrO_3$ increased with the increasing ZrO_2 particle sizes. Therefore, the oxygen flux due to the effect of Zr cation dissolution was greater than the influence of $SrZrO_3$ in the SCFZ membrane.

Effect of ZrO_2 particle sizes on structural stability

When ceramic membranes are used for oxygen separation, they are usually operated at high temperatures and are exposed to low oxygen partial pressures. Under such circum-

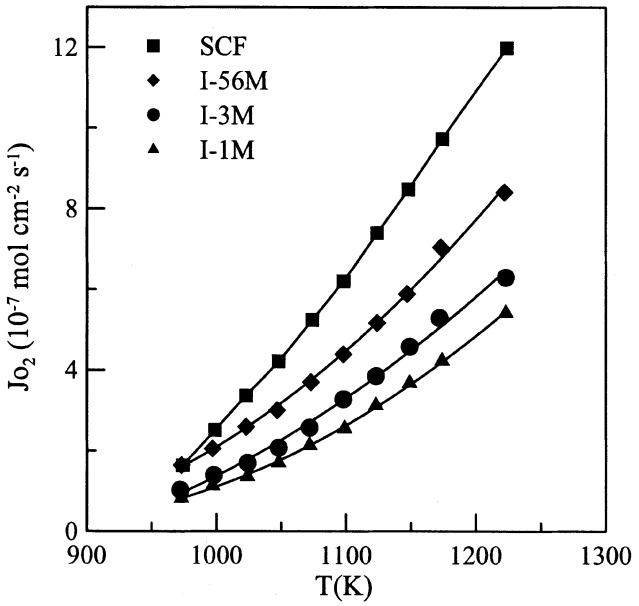

Figure 4. Temperature dependence of oxygen permeation fluxes through 1.78 mm SCF and SCFZ membranes added with different sizes of ZrO_2 prepared by method I, air/He.

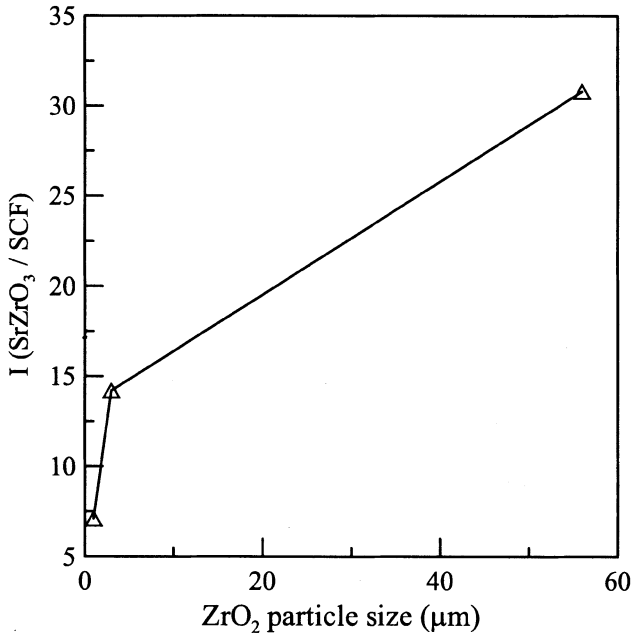

Figure 6. Semiquantitative analysis of the amount of secondary phase $SrZrO_3$ formed in the I-1 M, I-3 M, and I-56 M membranes.

stances, it is desirable that the structure is stable under the applied range of temperatures and oxygen partial pressures. Otherwise, undesirable vacancy trapping effects or volume changes associated with the development of a vacancy-ordered structure may occur. Figure 7 shows XRD patterns of 1,223 K–calcined SCF, I-1 M, I-3 M, and I-56 M powders annealed in helium at 973 K, 1,073 K and 1,123 K, respectively. When annealed at 973 K, the characteristic peak of SCF at $2\theta = 32°$ and 58° split, indicating a structure transition to the oxygen-vacancy ordered, orthorhombic phase of Sr_2CoFeO_5. As the sizes of added ZrO_2 decreased, the splitting of the peak weakened. When ZrO_2 particle sizes were reduced to 1 μm (I-1 M), it could stabilize its phase structure in the low-oxygen partial-pressure atmosphere. The results indicated that Zr dissolution enhanced the structure stability, and the stability increased as the decreasing ZrO_2 particle sizes decreased, due to an increasing Zr cation content in the B site of the SCF phase. The structure of the powders annealed at 1,073 K and 1,123 K were changed. This may indicate that more of the Zr cation was necessary in the SCF phase to maintain structural stability at these high temperatures. For powders prepared by method II, more of the Zr cation was dissolved compared with powders prepared by method I for the same added ZrO_2 sizes (Table 2), and, therefore, resulted in a more stable structure at a low-oxygen partial-pressure atmosphere. For example, the II-1M powders could maintain their stable structure even after annealed in helium at 1,123 K.

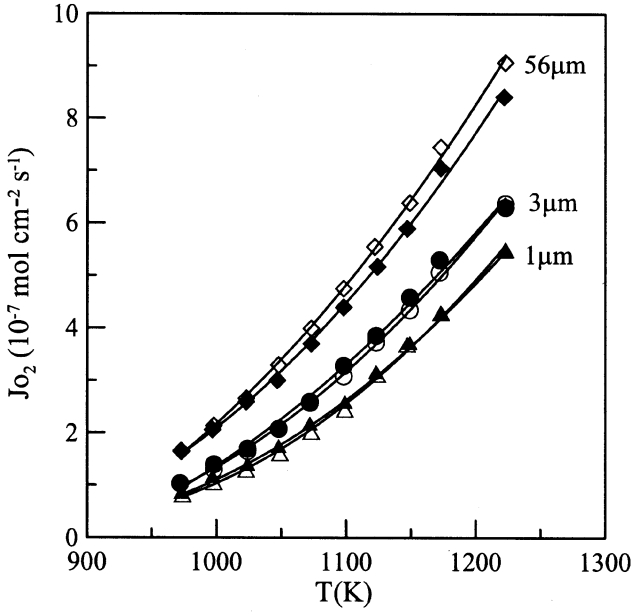

Figure 5. Comparison of oxygen flux of 1.78-mm SCFZ membranes by method I to method II: (◇) I-56 M; (◆) II-56 M; (○) I-3 M; (●) II-3 M; (△) I-1M; (▲) II-1 M.

Figure 8 summarizes the correlation between stability and the SCF-phase lattice parameters for the 1,123 K–annealed powders and membranes prepared by the two methods. It revealed that the stability increased with increasing lattice parameters, and only those samples with Zr cation dissolution reaching a certain value (corresponding lattice parameters higher than 3.867 Å) can retain their structural stability after annealing in helium at 1,123 K. It was also shown by the present study that ZrO_2 added with 1 μm by method II was the most effective way to attain Zr cation dissolution in the SCF phase.

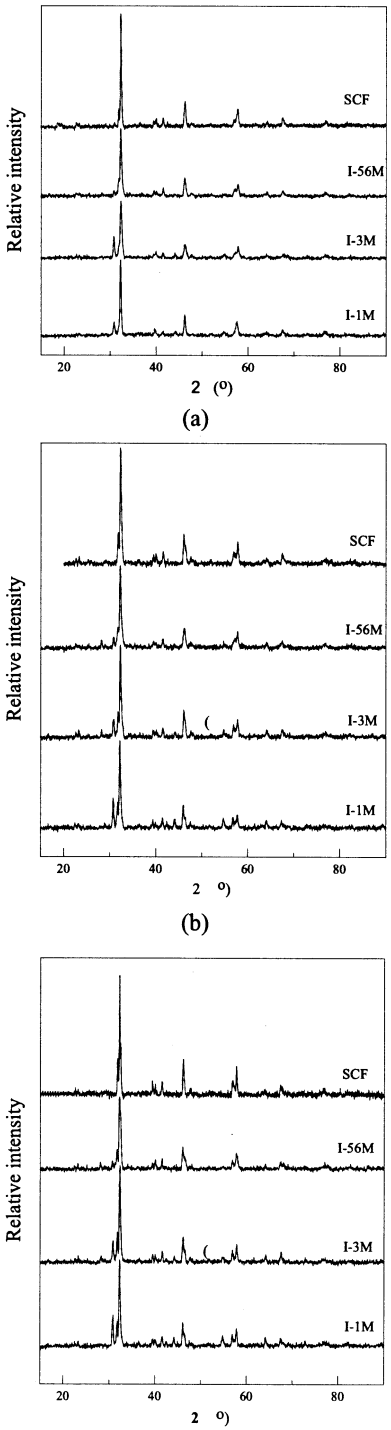

Figure 7. XRD patterns of 1,223 K calcined SCF, I-1 M, I-3 M, and I-56 M powders annealed in He at: (a) 973 K; (b) 1,073 K; (c) 1,123 K.

In the preceding study, the amount of added ZrO_2 was chosen randomly as 9 wt. % (Li et al., 1999), and although 9 wt. % ZrO_2 was enough to stabilize the SCF structure in a low-oxygen partial-pressure atmosphere, the formation of poor conducting phase $SrZrO_3$ might be unfavorable to oxygen flux of the membrane. It was shown in the earlier investigation that the properties of the materials were tailored by Zr cation dissolution, so it was possible to optimize the amount of ZrO_2 added to ensure a certain Zr content in the SCF phase to maintain the structural stability, but not to form the $SrZrO_3$ phase, which was unfavorable to oxygen permeation.

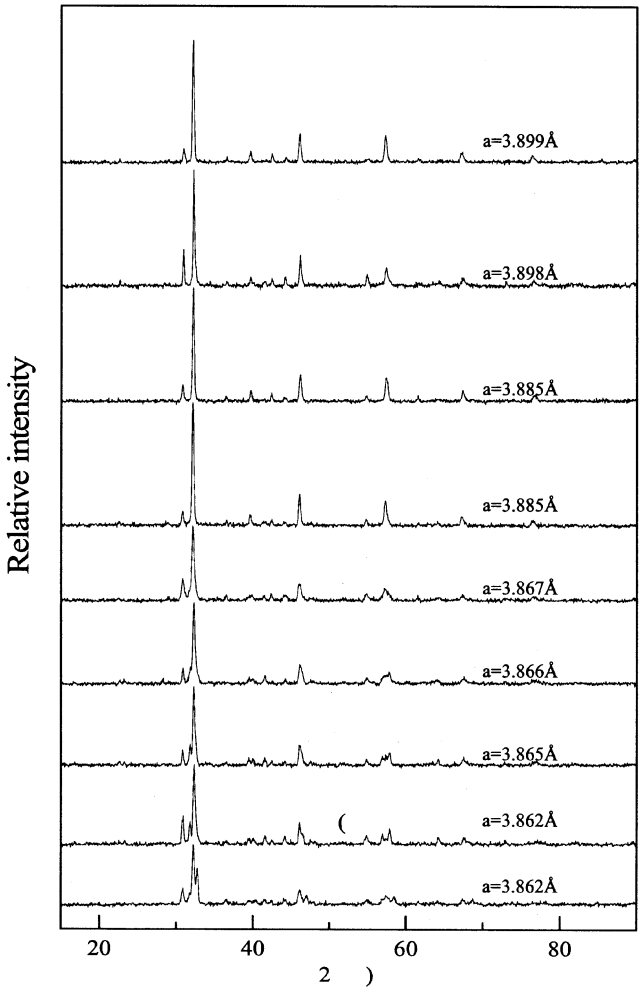

Figure 8. Correlation between stability and lattice parameter for samples annealed in He at 1,123 K.

Effect of the amount of ZrO_2 added on structure

Because ZrO_2 with a particle size of 1 μm added in method II was the most effective way to attain Zr cation dissolution in the SCF phase, we synthesized SCFZ powders with different amounts (0, 1, 3, 5, 7 and 9 wt. %) of ZrO_2 with a particle size of 1 μm added in method II, as described in the section titled "Sample preparation."

XRD patterns of the powders with ZrO_2 additions of 1–9 wt. % showed the existence of the SCF and $SrZrO_3$ phases. But for the sintered membranes, the second $SrZrO_3$ phase was reabsorbed into the perovskite for the compositions with $ZrO_2 \leq 7$ wt. % added. Therefore, the limit of solid solubility of ZrO_2 in the SCF membrane sintered at 1473 K was esti-

Table 4. EDX Analysis of SCF Phases for the SCFZ Membranes Added with Different Amount of ZrO_2

ZrO_2 Addition (wt. %)	Composition (mol %)			
	Sr	Co	Fe	Zr
1	42.57	20.33	35.95	1.16
3	44.35	18.53	34.12	2.99
5	44.84	17.10	33.59	4.46
7	41.03	20.93	31.82	6.23
9	42.93	16.31	32.50	8.26

mated to be about 7 wt. %. A small amount of Co_3O_4 was also detected by XRD for samples added with ≥ 3 wt. % ZrO_2 (the Co_3O_4 phase was detected in all samples by EDX analysis, and its amount in samples with $ZrO_2 \leq 1$ wt. % added was so small that it was beyond the sensitivity threshold of XRD analysis), and the intensity of it increased as the amount of ZrO_2 increased. The formation of this phase may be attributed to two actions: the segregation of Co at high temperature (Takeda et al., 1986) and the precipitation of Co to maintain the stoichiometry because of Zr dissolution. The presence of these phases in the membranes was confirmed by SEM-EDX analysis for the sintered membrane. Besides, EDX analysis performed on the region corresponding to the SCF phase (see Table 4) showed that the compositions of Sr, Co, Fe, and Zr in five membranes with ZrO_2 additions of 1, 3, 5, 7, and 9 wt. % were 1:0.48:0.84:0.027, 1:0.42:0.77:0.067, 1:0.38:0.75:0.099, 1:0.51:0.77:0.15, and 1:0.38:0.76:0.19, respectively, indicating that the Zr content in the SCF phase increased directly with the amount of ZrO_2 added.

Effect of the amount of ZrO_2 added on structural stability

To study the phase behavior under the low-oxygen partial-pressure atmospheres, SCFZ membranes with various amounts of ZrO_2 additions were crushed and annealed in helium at 1,123 K for 3 h and then subjected to XRD analysis. The crystal structure of samples added with 0 and 1 wt. % ZrO_2 had changed from cubic phase to an oxygen-vacancy ordered phase. The structural stability of the materials improved with the increasing amount of ZrO_2 added due to increasing amount of Zr dissolution in the SCF phase, and when the ZrO_2 addition was ≥ 3 wt. %, samples could maintain their phase structure after being annealed in helium.

In order to study the structure phase transition in more detail, TG and DSC were carried out for samples with and without the addition of ZrO_2. The results are shown in Figure 9, in which samples with 1 wt. % and 7 wt. % ZrO_2 additions are taken as examples. In the case of samples with ZrO_2 additions of 0 and 1 wt. %, small endothermic peaks centered at about 1,098 K were found on heating, and the exothermic DSC peaks were observed on cooling. Obviously, these changes in heat were associated with the order–disorder phase transition between the brownmillerite and cubic perovskite phases (Liu et al., 1996; Kruidhof et al., 1993; Kim et al., 1997), which was in agreement with the structure transition detected by XRD analysis. While for samples with ZrO_2 additions of >1 wt. %, only endothermic peaks were observed on heating, and it became obvious with the increasing amount of ZrO_2 added. The endothermic peak observed for samples with ZrO_2 additions of >1 wt. % were most probably due to the decomposition of Co_3O_4 rather than the order–disorder phase transition, because the order–disorder phase transition was reversible (Liu et al., 1996; Kim et al., 1997), while only endothermic peaks were found on heating for samples with ZrO_2 additions of >1 wt. %.

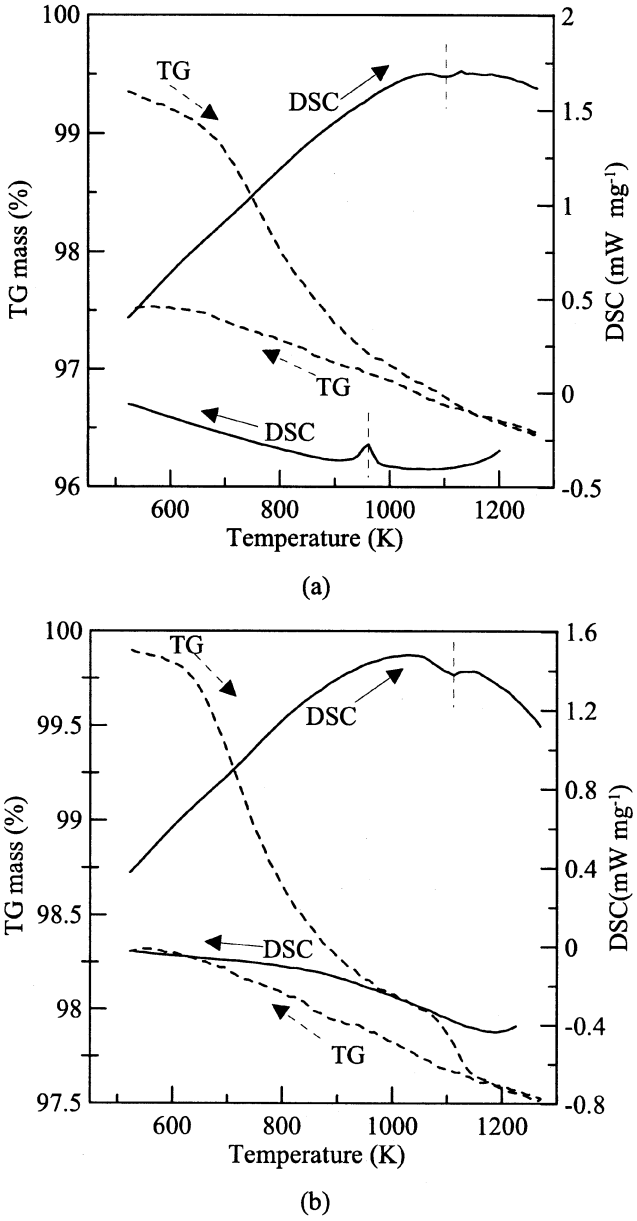

Figure 9. TG-DSC curves of samples with ZrO_2 additions of (a) 1 wt. % and (b) 7 wt. % in nitrogen atmosphere (heating and cooling rates 10 K/min).

Effect of the amount of ZrO_2 added on oxygen permeation

The temperature dependence of oxygen flux through SCFZ membranes is shown in Figure 10 for the ZrO_2 additions of 0, 1, 3, 5, 7, and 9 wt. %. The oxygen flux was found to decrease monotonically with the increasing amount of ZrO_2 added. As shown in Figure 10, two activation energies for

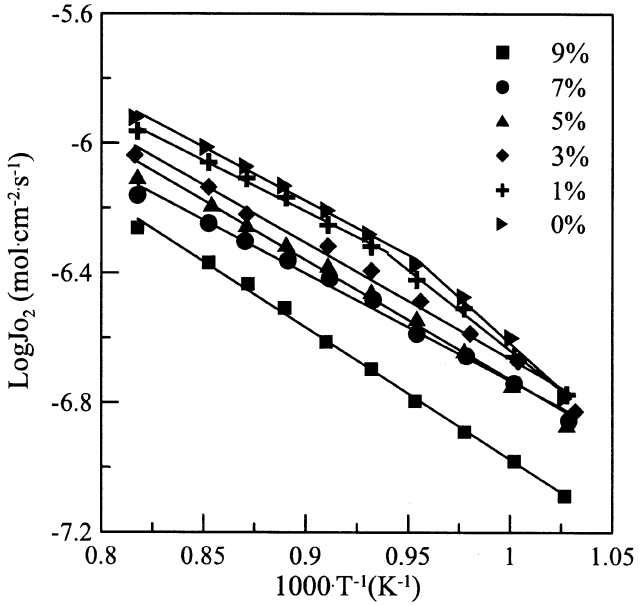

Figure 10. The temperature dependence of oxygen permeation flux through 1.78 mm SCFZ membranes with varying ZrO_2 additions, air/He.

oxygen permeation in the 973–1,223 K range were observed for the compositions with ZrO_2 additions of < 3 wt. %, which was related to the order–disorder transition of oxygen vacancies (Kruidhof et al., 1993; Qiu et al., 1995). In contrast, single activation for oxygen permeation was observed for samples with ZrO_2 addition > 3 wt. %. The results were in accordance with the XRD and DSC analysis mentioned earlier. From the dependence of stability and oxygen permeability on the amount of ZrO_2 added described earlier, the optimum amount of ZrO_2 addition was to greatly improve the structural stability without deleteriously affecting the oxygen permeability has been identified as 3 wt. %.

Conclusions

The structure, oxygen permeation, and stability of $SrCo_{0.4}Fe_{0.6}O_{3-\delta}$ (SCF) oxide can be changed by adding ZrO_2 of different particle sizes and different addition amounts. The particle sizes (1, 3, 56 μm) and the amounts (1, 3, 5, 7, 9 wt. %) of ZrO_2 added were selected for this study. Element analysis revealed that a considerable diffusion of Zr cation into the SCF phase occurred at high temperatures, resulting in a lattice expansion of SCF. The amount of Zr cation dissolution increased with decreasing particle sizes and increasing amounts of ZrO_2 added. The solid solubility limit of ZrO_2 in the SCF membrane at 1,473 K was estimated by XRD and SEM-EDX analysis to be about 7 wt. %. Oxygen permeation fluxes decreased, while structural stability increased with decreasing ZrO_2 sizes and increasing amounts of ZrO_2 added due to the increasing amount of Zr cation in the B site of SCF. To sustain the structural stability of SCF in a low-oxygen partial-pressure atmosphere, doping a certain amount of Zr cation in the SCF phase was an effective route, and the optimum amount of ZrO_2 added that would greatly improve the structural stability without deleteriously affecting the oxygen permeability has been identified as 3 wt. % using ZrO_2 with a particle size of 1 μm.

Acknowledgments

This work was supported by the National Natural Science Foundation of China (NNSFC, No. 20125618) and the Key Laboratory of Chemical Engineering and Technology of Jiangsu Province.

Literature Cited

Balachandran, U., J. T. Dusek, S. M. Sweeney, R. L. Mieville, P. B. Poppel, M. S. Kleefisch, S. Pei, T. P. Kobylinski, C. A. Udovich, and A. C. Bose, "Dense Ceramic Membranes for Partial Oxidation of Methane to Syngas," *Appl. Catal. A: Gen.*, **133**, 19 (1995).

Foster, E. P., P. J. A. Tijm, and D. L. Bermett, "Advanced Gas-to-Liquids Process for Syngas and Liquid-Conducting Membrane Reactor," *Stud. Surf. Sci. Catal.*, **119**, 867 (1998).

He, H. P., X. J. Huang, and L. Q. Chen, "The Effects of Dopant Valence on the Structure and Electrical Conductivity of $LaInO_3$," *Electrochim. Acta*, **46**, 2871 (2001).

Kharton, V. V., E. N. Naumovich, and A. V. Nikolaev, "Materials of High-Temperature Electrochemical Oxygen Membranes," *J. Membr. Sci.*, **111**, 149 (1996).

Kharton, V. V., A. V. Kovalevsky, A. P. Viskup, F. M. Figueiredo, A. A. Yaremchenko, E. N. Naumovich, and F. M. B. Marques, "Oxygen Permeability of $Ce_{0.8}Gd_{0.2}O_{2-\delta}$-$La_{0.7}Sr_{0.3}MnO_{3-\delta}$ Composite Membranes," *J. Electrochem. Soc.*, **147**, 2817 (2000).

Kim, S., Y. L. Yang, R. Christoffersen, and A. J. Jacobson, "Oxygen Permeation, Electrical Conductivity and Stability of the Perovskite Oxide $La_{0.2}Sr_{0.8}Cu_{0.4}Co_{0.6}O_{3-x}$," *Solid State Ionics*, **104**, 57 (1997).

Kruidhof, H., H. J. Boumeester, R. H. E. v. Doorn, and A. J. Burggraaf, "Influence of Order-Disorder Transitions on Oxygen Permeability Through Selected Nonstoichiometric Perovskite-Type Oxides," *Solid State Ionics*, **63–65**, 816 (1993).

Li, S. G., W. Q. Jin, P. Huang, N. P. Xu, J. Shi, Z. C. Hu, E. A. Payzant, and Y. H. Ma, "Perovskite-Related ZrO_2-Doped $SrCo_{0.4}Fe_{0.6}O_{3-\delta}$ Membrane for Oxygen Permeation," *AIChE J.*, **45**, 276 (1999).

Liu, L. M., T. H. Lee, L. Qiu, Y. L. Yang, and A. J. Jacobson, "A Thermogravimetric Study of Phase Diagram of Strontium Cobalt Iron Oxide, $SrCo_{0.8}Fe_{0.2}O_{3-\delta}$," *Mater. Res. Bull.*, **31**, 29 (1996).

Lu, Y., A. G. Dixon, W. R. Moser, Y. H. Ma, and U. Balachandran, "Oxygen-Permeable Dense Membrane Reactor for the Oxidation Coupling of Methane," *J. Membr. Sci.*, **170**, 27 (2000).

Pei, S., M. S. Kleefisch, T. P. Kobylinski, J. Faber, C. A. Udovich, V. Zhang-Mccoy, B. Dabrowski, U. Balachandran, R. L. Mieville, and R. B. Poeppel, "Failure Mechanisms of Ceramic Membrane Reactors in Partial Oxidation of Membrane to Synthesis Gas," *Catal. Lett.*, **30**, 201 (1995).

Poulsen, F. W., and N. van der Puil, "Phase Relations and Conductivity of Sr-Zirconates and La-Zirconates," *Solid State Ionics*, **53**, 777 (1992).

Prado, F., T. Armstrong, A. Caneiro, and A. Manthiram, "Structural Stability and Oxygen Permeation Properties of $Sr_{3-x}La_x$-$Fe_{2-y}Co_yO_{7-\delta}$ ($0 \le x \le 0.3$ and $0 \le y \le 1.0$)," *J. Electrochem. Soc.*, **148**, J7 (2001).

Qiu, L., T. H. Lee, L. M. Liu, Y. L. Yang, and A. J. Jacobson, "Oxygen Permeation Studies of $SrCo_{0.8}Fe_{0.2}O_{3-\delta}$," *Solid State Ionics*, **76**, 321 (1995).

Shannon, R. D., and C. T. Prewitt, "Effective Ionic Radii in Oxides and Fluorides," *Acta Cryst.*, **B25**, 925 (1969).

Stevenson, J. W., T. R. Armstrong, R. D. Carmeim, L. R. Pederson, and W. J. Weber, "Electrochemical Properties of Mixed Conducting Perovskites $La_{1-x}M_xCo_{1-y}$ $Fe_yO_{3-\delta}$ (M = Sr, Ba, Ca)," *J. Electrochem. Soc.*, **143**, 2722 (1996).

Takeda, Y., R. Kanno, T. Takada, O. Yamamoto, M. Takano, and Y. Bando, "Phase Relation and Oxygen-Non-Stoichiometry of Perovskite-like Compound $SrCoO_x$ ($2.29 \le x \le 2.80$)," *Z. Anorg. Allg. Chem.*, **9–10**, 259 (1986).

Ten Elshof, J. E., H. J. M. Bouwmeester, and H. Verweij, "Oxygen

Transport Through $La_{1-x}Sr_xFeO_{3-\delta}$ Membranes, I. Permeation in Air/He Gradient," *Solid State Ionics*, **81**, 97 (1995).
Tsai, C.-Y., A. G. Dixon, Y. H. Ma, W. R. Moser, and M. R. Pascucci, "Dense Perovskite, $La_{1-x}A_xFe_{1-y}Co_yO_{3-\delta}$ (A = Ba, Sr, Ca), Membrane Synthesis, Applications, and Characterization," *J. Amer. Ceram. Soc.*, **81**, 1437 (1998).
Weppner, W., "Materials and Concepts for Solid State Electromechanical Devices," *Fast Ion Transport in Solids, NATO ASI Series E, Applied Sciences Vol.*, B. Scrosati, A. Magistris, C. M. Mari, and G. Mariotto, eds., Klewer, Dordrecht, The Netherlands, p. 9 (1992).
Wiik, K., C. R. Schmidt, S. Faaland, S. Shamsili, M.-A. Einarsrud, and T. Grande, "Reaction Between Strontium-Substituted Lanthanum Manganite and Yttria-Stabilized Zirconia: I, Powder Samples," *J. Amer. Cream. Soc.*, **82**, 721 (1999).
Xu, S. J., and W. J. Thomson, "Perovskite-Type Oxide Membranes for the Oxidative Coupling of Methane," *AIChE J.*, **43**, 2731 (1997).
Yang, L., X. H. Gu, L. Tan, W. Q. Jin, L. X. Zhang, and N. P. Xu, "Oxygen Transport Properties and Stability of Mixed-Conducting ZrO_2-Promoted $SrCo_{0.4}Fe_{0.6}O_{3-\delta}$ Oxides," *Ind. Eng. Chem. Res.*, **41**, 4273 (2002).
Zeng, Y., Y. S. Lin, and S. L. Swartz, "Perovskite-Type Ceramic Membrane: Synthesis, Oxygen Permeation and Membrane Reactor Performance for Oxidative Coupling of Methane," *J. Membr. Sci.*, **150**, 87 (1998).

Manuscript received Sept. 17, 2002, and revision received Mar. 6, 2003.